Mapping Exoplanets

Nicolas B. Cowan and Yuka Fujii

Contents

Abstract

The varied surfaces and atmospheres of planets make them interesting places to live, explore, and study from afar. Unfortunately, the great distance to exoplanets makes it impossible to resolve their disk with current or near-term technology. It is still possible, however, to deduce spatial inhomogeneities in exoplanets provided that different regions are visible at different times—this can be due to rotation, orbital motion, or occultations by a star, planet, or moon. Astronomers have so far constructed maps of thermal emission and albedo for short period

N. B. Cowan (✉)
McGill University, Montréal, QC, Canada
e-mail: nicolas.cowan@mcgill.ca

Y. Fujii
National Astronomical Observatory of Japan, Mitaka, Tokyo, Japan
e-mail: yuka.fujii@nao.ac.jp

giant exoplanets. These maps constrain atmospheric dynamics and cloud patterns in exotic atmospheres. In the future, exo-cartography could yield surface maps of terrestrial planets, hinting at the geophysical and geochemical processes that shape them.

Introduction

Astronomy often involves studying objects so distant that they remain unresolved point sources with even the largest telescopes. Exoplanets are particularly difficult to study, because they are small compared to other astronomical objects. The diffraction limit dictates that resolving the disk of an Earth-sized planet at 10 pc requires a telescope—or array of telescopes—at least 25 km across at optical wavelengths, or 500 km across in the thermal infrared. Short of building a large interferometer to spatially resolve the disks of exoplanets, we must rely on chance and astronomical trickery to map their atmospheres and surfaces.

We expect planets to have spatial inhomogeneities: left to their own devices, atmospheres are subject to instabilities that produce spatially and temporally varying temperature, composition, and aerosols. Moreover, planets orbiting a star are further subject to asymmetric radiative forcing from their star, leading to diurnal (day–night) and seasonal (summer–winter) variations. Lastly, the surface of a planet may have a heterogeneous character due to, e.g., plate tectonics or volcanism.

Although part of the motivation to map exoplanets is simply to know what they look like, there are undoubtedly cases where understanding a planet requires understanding the diversity of its different regions. On a short-period planet, for instance, the hot dayside atmospheres may have atomic and partially ionized gas, while the nightside may be hundreds to thousands of degrees cooler, often shrouded in clouds and sometimes entirely airless. Interpreting the disk-integrated light of a heterogeneous planet with a one-dimensional model is misleading (e.g., Feng et al. 2016). More importantly, the intrinsic climate of a planet is affected by its spatial inhomogeneities (Zhang 2023a,b; Zhang et al. 2023). We would therefore like to map the atmospheres and surfaces of exoplanets.

Mapping Basics

This chapter covers the analysis of planetary light, be it thermal radiation or reflected starlight. Planetary light can be separated from starlight temporally (Charbonneau et al. 2005; Deming et al. 2005), spatially (Marois et al. 2008), or spectrally (Brogi et al. 2012). Transmission mapping is also briefly described below.

It is possible to map the surface of an unresolved object as long as we don't always see the same parts of it—the resulting changes in brightness can be detected across astronomical distances. We are therefore able to tease out spatial information about a planet based on its time-variable brightness, provided we know something about the viewing geometry. There are three ways in which our view of an exoplanet
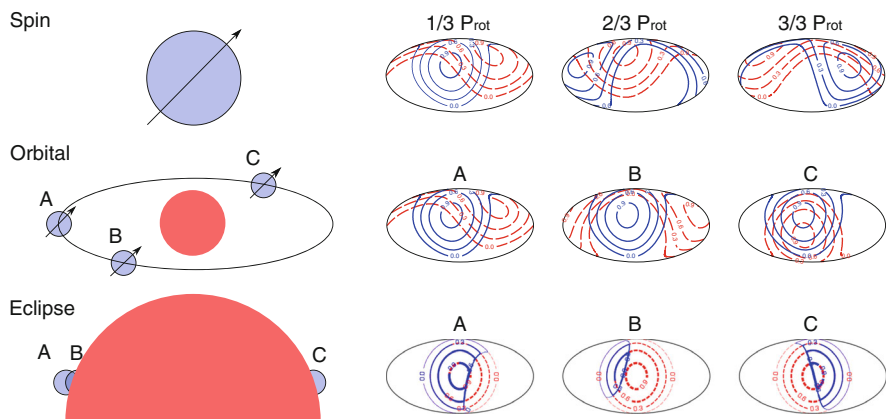
Fig. 1 The visibility (blue contours) and illumination (red contours) at three times for the different exoplanet mapping techniques: rotational mapping (top), orbital mapping (middle), and eclipse mapping (bottom). The inclination is 60° in the top two panels, and in the middle panel, the planetary obliquity is 45°. For thermal emission, the convolution kernel is proportional to the visibility, while for diffuse reflected light, the kernel is proportional to the product of visibility and illumination (see the Kernel section below). When the planet is unoccluded (top two rows), the nonzero regions of the visibility and illumination are each hemispheres, making the nonzero portion of the reflection kernel a *lune*. For the occultation geometry shown in the bottom row, the planet is slowly rotating, so that essentially the same hemisphere is facing the observer before and after the occultation

can change: rotation of the planet, changes in its position with respect to its star, and occultations by another object (Fig. 1).

Rotational mapping is possible, because at any given time, we only see light from at most a hemisphere and as the planet spins on its own axis, different atmospheric and surface features rotate in and out of view. Orbital mapping with reflected light is possible due to the changing illumination pattern as the planet orbits its star. Occultation mapping, on the other hand, requires a second object to obscure part of the planet—the host star is the most likely culprit—hence changing our view and the system's overall flux. In practice, multiple sources of variability can be present in a single data set: phase variations are generally accompanied by rotation of the planet, and occultations are necessarily accompanied by orbital motion.

Transmission Mapping

It is also possible to glean spatial information about an exoplanet's atmosphere when it transits in front of its host star: transmission mapping or transit mapping. Transmission mapping shares some concepts with emission and reflection mapping, so is briefly described here. Transmission mapping relies on two geometrical facts: (1) only part of the planetary limb is backlit during transit ingress and egress, and (2) the planetary limb probed in transmission moves on the planet during a transit.

At the start of transit ingress, only the western (leading) limb of the planet is in front of the star and contributes to the transmission spectrum; likewise, the end of egress is only sensitive to the eastern (trailing) limb of the planet. Such transmission mapping has been proposed for detecting the difference in atmospheric scale height (Dobbs-Dixon et al. 2012), winds (Louden and Wheatley 2015), and aerosols (Kempton et al. 2017; Powell et al. 2019) near the eastern and western terminators. Many codes have been developed to perform such transmission mapping (Espinoza and Jones 2021; MacDonald and Lewis 2022; Grant and Wakeford 2023). The ingress-egress asymmetry is most marked for planets that are large compared to their star; the best spatial resolution could be obtained for a giant planet orbiting a white dwarf (e.g., Vanderburg et al. 2020). Transit mapping is conceptually similar to eclipse mapping but is very sensitive to the limb darkening of the star. Transmission mapping has already been performed with ground-based high-resolution spectroscopy (Ehrenreich et al. 2020). Even in the middle of transit, high-resolution data can differentiate between the blue-shifted eastern limb and the red-shifted western limb (Boucher et al. 2023; Klein et al. 2024), analogous to Doppler imaging.

Moreover, the planet will rotate during the transit, i.e., the planetary limb does not exactly coincide with the day–night terminator. In fact, the limb only corresponds to the day–night terminator when the planet is in the center of the stellar disk, which never occurs for a nonzero impact parameter. At the start of transit, the limb runs on the dayside of the eastern terminator and on the nightside of the western terminator, and vice versa at the end of transit. The angle between the limb and terminator is proportional to the angular size of the star as seen from the planet and is therefore most important for ultrashort period planets (Nguyen et al. 2020). If a rocky planet has a negligible atmosphere, then topographical features may rotate in and out of view during the transit (McTier and Kipping 2018). Transmission mapping of exoplanets is an exciting growth area, but the remainder of this review focuses on mapping exoplanets using light emitted or reflected by the planets themselves.

Mapping Formalism

Exo-cartography is an *inverse problem*, as opposed to the *forward problem* of predicting the spectrum of a planet based on its surface and atmospheric properties. The usual approach to an inverse problem is to solve the forward problem many times with varying parameters to see which ones best match the observations.

State-of-the-art forward modeling involves, at the very least, detailed radiative transfer calculations and hence is not useful for solving the inverse problem (Robinson et al. 2011). One of the necessities of tackling the inverse problem is therefore making judicious simplifications. Adopting the notation of Cowan et al. (2013), the exo-cartography forward problem is approximated as

$$F(t) = \oint K(\theta, \phi, t) M(\theta, \phi) d\Omega, \tag{1}$$

where $F(t)$ is the observed flux, or lightcurve, $K(\theta, \phi, t)$ is the convolution kernel, $M(\theta, \phi)$ is the top-of-atmosphere planet map, θ and ϕ are planetary co-latitude and longitude, respectively, the differential solid angle is $d\Omega = \sin\theta d\theta d\phi$ for a spherical planet, and $\oint d\Omega$ is the integral over the entire planet. Although F stands for "flux," the units of $F(t)$ depend on the situation and chosen normalization: planetary flux, planet/star flux ratio, reflectance, apparent albedo, etc.

Arguably, the most important simplification is assuming a static map, $\partial M/\partial t = 0$, as it is generally intractable to map the surface of an unresolved planet when that map is changing. One can map a slowly varying planet, e.g., large-scale cloud patterns on Earth evolve slowly compared to the planet's rotation (Kawahara and Masuda 2020; Teinturier et al. 2022), and some eccentric planets may still be amenable to eclipse mapping, despite seasonal variations. Beyond these exceptions, one must adopt a parameterized time-variable map, $M(\theta, \phi, t)$. For example, phase curves of eccentric hot Jupiters have been fitted with energy balance models (Lewis et al. 2013; de Wit et al. 2016; Dang et al. 2022). Finally, Cowan et al. (2017) showed that for planets on circular, edge-on orbits, one can infer a time-variable map based on the presence of odd harmonics; nonetheless, this is a far cry from mapping the changing surface of a planet.

Barring a changing map, time variations in flux come in through the kernel. If there are no occultations, then the changing sub-observer and substellar locations dictate the time variability of the kernel and hence the time variations in observed flux.

The Inverse Problem

Inverse problems are often under-constrained, and exo-cartography is no exception: nonzero maps can produce flat lightcurves, a so-called nullspace, and different maps sometimes produce identical nontrivial lightcurves. These pitfalls represent the loss of information: attempts to map distant objects suffer from formal degeneracies, even in the limit of noiseless observations.

If the orientation of a planet is not known a priori, then the problem is even more challenging, because the kernel is a function of one or more unknown parameters: spin frequency, spin orientation, etc. Nonetheless, it has been demonstrated in numerical experiments that one can extract a planet's spin (rotation rate, obliquity, and its direction) from reflected lightcurves (Pallé et al. 2008; Oakley and Cash 2009; Kawahara and Fujii 2010, 2011; Fujii and Kawahara 2012; Schwartz et al. 2016; Kawahara 2016; Farr et al. 2018; Nakagawa et al. 2020) or from thermal lightcurves (Gaidos and Williams 2004; Gómez-Leal et al. 2012; Cowan et al. 2012b, 2013). A similar formalism has been developed for imaging exoplanets with a solar gravitational lens (Toth and Turyshev 2023).

Exoplanets can be mapped in monochrome using single-band photometry, or using spectrally resolved data to produce maps at each wavelength. It is often more insightful, however, to assume that the lightcurves are correlated due to viewing geometry, molecular absorption, or surface spectra. With high spectral resolution,

for example, the signal is in the time-variable mean molecular line shape. The interested reader is pointed to the excellent review of high-resolution atmospheric characterization (Birkby 2018) and note that much work remains to be done in extracting spatial information from high-resolution data. The inverse problem of mapping a planet using template spectra—let alone retrieving intrinsic surface colors and spectra—based on multiband photometry or time-resolved spectroscopy is beyond the scope of this review but has been considered in the literature both in the context of reflected light (Cowan et al. 2009, 2011; Fujii et al. 2010, 2011, 2017; Cowan and Strait 2013; Kawahara 2020) and thermal emission (Kostov and Apai 2013; Buenzli et al. 2014; Stevenson et al. 2014; Feng et al. 2016; Irwin et al. 2020; Changeat and Al-Refaie 2020; Cubillos et al. 2021).

Basis Maps and Basis Lightcurves

The exo-cartography inverse problem boils down to fitting observed lightcurves. One can use orthonormal basis maps, e.g., spherical harmonics,

$$\frac{1}{4\pi} \oint M_1(\theta, \phi) M_2(\theta, \phi) d\Omega = \delta_{12}, \tag{2}$$

and repeatedly solve the forward problem in order to fit an observed lightcurve, or one can use orthonormal basis lightcurves, e.g., a Fourier series or eigencurves (Rauscher et al. 2018),

$$\frac{1}{P} \int_0^P L_1(t) L_2(t) dt = \delta_{12}, \tag{3}$$

to directly fit the observed lightcurve, then reconstruct the associated map and its uncertainties in post-processing. Sometimes, orthonormal basis maps produce orthonormal basis lightcurves, and the problem is particularly tidy, as for rotational thermal mapping (Cowan and Agol 2008; Cowan et al. 2013). Usually, however, the adopted basis maps do not produce orthogonal lightcurves, and vice versa.

There are two broad classes of map parameterizations: global (e.g., spherical harmonics) and local (e.g., pixels). Examples of both basis maps are shown in Fig. 2. The optimal basis maps will depend on viewing geometry, expected map geometry, and the nature of the data (cf. Keating et al. 2019; Beatty et al. 2019). In general, spherical harmonics are better for rotational mapping, smoothly varying maps, and full phase coverage. Pixels are preferable for eclipse mapping, sharp features, or partial phase coverage. Apai et al. (2017) introduced hybrid basis maps to fit rotational lightcurves of brown dwarfs: zonal bands harboring sinusoidal waves.

It is advisable to adopt a basis for which some maps are constrained and others are unambiguously in the nullspace, as it makes degeneracies easier to track down. As with many inverse problems, priors on the model parameters can help stabilize
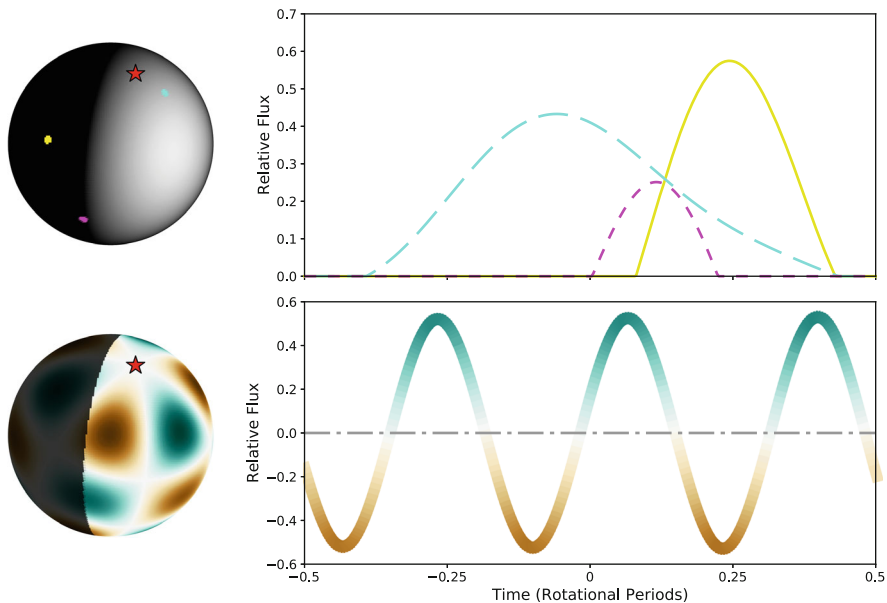
Fig. 2 Basis maps and their reflected lightcurves. Examples of δ-maps (top) and a spherical harmonic map (bottom). For the δ-functions of the top panel, the resulting lightcurves are simply the value of the kernel at a particular location on the planet as a function of time, making them trivial to compute; small pixels would have approximately the same lightcurves. For the spherical harmonic map in the bottom panel, note that the resulting lightcurve is conveniently sinusoidal. The red star in each image denotes the north planetary pole, and the planet rotates to the east. (Figure from J.C. Schwartz (private communication))

fits, especially when the data are noisy. For exo-cartography, this takes the form of enforcing map positivity (Keating and Cowan 2017; Farr et al. 2018), regularization to favor smoothness between pixels (e.g., Knutson et al. 2007; Kawahara and Fujii 2010, 2011; Fujii and Kawahara 2012), suppressing power in high-order modes with a sharp cutoff (e.g., Cowan and Agol 2008; Majeau et al. 2012), or a Gaussian process (Farr et al. 2018; Kawahara and Masuda 2020; Luger et al. 2021).

Pixels and Slices

An intuitive approach to mapping is to pixelize the planetary surface. The most general pixelization scheme is two-dimensional, for example, a latitude–longitude grid or Hierarchical Equal Area isoLatitude Pixelization (HEALPix), but more exotic schemes have been developed for occultation mapping (Louden and Kreidberg 2018). Pixels are useful if the kernel moves or changes its shape in more than one direction, e.g., eclipse mapping or rotational reflected light curves at multiple orbital phases.

Denoting the intensity of the ith pixel by m_i, we may express an arbitrary map as

$$M(\theta, \phi) = \sum m_i M_i(\theta, \phi), \tag{4}$$

where the basis maps are

$$M_i(\theta, \phi) = \begin{cases} 1 & \text{if } \{\theta, \phi\} \in \ i\text{th pixel}, \\ 0 & \text{otherwise.} \end{cases} \tag{5}$$

A small pixel is well approximated by a δ-function at its center. Although δ-functions are terrible for decomposing continuous maps, they have the advantage of being trivial to integrate (Haggard and Cowan 2018):

$$F_{\theta\phi}(t) = \oint K(\theta', \phi', t)\delta(\theta' - \theta, \phi' - \phi)d\Omega' = K(\theta, \phi, t). \tag{6}$$

For rotational mapping, latitudinal information is difficult to extract, so it is often reasonable to consider a map consisting of uniform slices, like a beach ball. This situation includes rotational mapping in the thermal infrared (Knutson et al. 2007) and rotational mapping of reflected light at a fixed orbital phase (Cowan et al. 2009).

Spherical Harmonics

A continuous albedo map, $M(\theta, \phi)$, may be decomposed into spherical harmonics:

$$M(\theta, \phi) = \sum_{l=0}^{\infty} \sum_{m=-l}^{l} C_l^m Y_l^m(\theta, \phi), \tag{7}$$

where the coefficients are

$$C_l^m = \frac{1}{4\pi} \oint M(\theta, \phi) Y_l^m(\theta, \phi)d\Omega. \tag{8}$$

It is difficult to extract latitudinal information from purely rotational variations (the little that can be squeezed out is described by Cowan et al. 2013, 2017). It is expedient in such cases to adopt sinusoidal basis maps (Cowan and Agol 2008), essentially spherical harmonics with $m = l$.

The Kernel

The kernel is the equivalent to the vertical contribution function in 1D atmospheric radiative transfer (Kawahara and Fujii have used "weight" instead of "kernel"). By definition, the kernel must move over the planet in order for exo-cartography to

be possible. The shape of the kernel, however, is constant for rotational mapping and thermal phase mapping. For such a static kernel, some maps are always in the nullspace, leading to severe degeneracy in the inverse problem (Cowan et al. 2013). If the shape of the kernel changes with time, then maps need not remain in the nullspace, e.g., eclipse mapping (Challener and Rauscher 2023), or reflected-light mapping involving both rotation and orbital motion (Haggard and Cowan 2018). The degeneracy-busting power of a changing kernel is analogous to how a changing antenna pattern reduces the degeneracy in the location of a radio source on the sky.

Thermal Emission

For diffuse thermal emission, the kernel is simply the normalized visibility:

$$K(\theta, \phi, t) = \frac{1}{\pi} V(\theta, \phi, t), \tag{9}$$

where the visibility, V, is unity at the sub-observer location (the center of the planetary disk as seen by the observer), drops as the cosine of the angle from the sub-observer location if limb darkening can be neglected, and is zero on the far side of the planet or any part of the planet hidden from view by an occulting object. Cowan et al. (2013) used this kernel to derive analytic orbital/rotational lightcurves for spherical harmonic basis maps and Luger et al. (2019a) did the same for occultations.

Due to the unchanging kernel shape for rotational or orbital thermal mapping, a large fraction of spherical harmonics are in the nullspace, limiting the fidelity of retrieved maps. A common strategy is to ignore basis maps in the nullspace, setting their amplitude to zero in fits (Cowan and Agol 2008). But this strategy can sometimes produce retrieved maps that appear to have regions of negative flux, an artifact of the band-limited deconvolution. The solution is to fit for more basis maps—including those in the nullspace: immeasurable fitted parameters may help the map remain everywhere positive (Keating et al. 2019). Such hidden variables can be further constrained by a regularization scheme or Gaussian process. Indeed, the most general and robust approach to mapping is likely a high-order orthogonal map expansion—many spherical harmonics or pixels—embedded in a hierarchical model (Farr et al. 2018; Luger et al. 2021). If the prospect of fitting unseen and unknowable parameters by relying on priors is daunting, rest assured that you can often obtain a good fit and reasonable map by adopting an altogether different parameterization, such as slices or pixels (Beatty et al. 2019).

Reflected Light

For diffuse reflected light (a.k.a. Lambertian reflection), the kernel is the product of visibility and illumination:

$$K(\theta, \phi, t) = \frac{1}{\pi} V(\theta, \phi, t) I(\theta, \phi, t), \tag{10}$$

where the visibility is defined as above and the illumination I is unity at the substellar location (the center of the planetary disk as seen from the star), drops

as the cosine of the angle from the substellar location, and is zero on the night side of the planet or any part of the planet in the shadow of another object (e.g., an eclipsing planet or moon). Analytic reflected lightcurves have so far been derived for spherical harmonic maps at full phase (Russell 1906), for tidally locked, edge-on geometry (Cowan et al. 2013), for the general case of an unocculted planet (Haggard and Cowan 2018), and finally including occultations (Luger et al. 2022). Extending this framework to polarized reflected light is beyond the scope of this review but would undoubtedly yield useful constraints on cloud and surface properties (for a review of exoplanet polarimetry, see Wiktorowicz and Stam 2015).

The Lambertian scattering approximation is suitable for mapping gibbous planets (Fujii and Kawahara 2012), but preferential back scattering can be important at full phase, while forward scattering and specular reflection are important at crescent phases (Robinson et al. 2010). If specular reflection is the dominant form of reflection, then the kernel is approximately a δ-function at the location of the glint spot, making the forward problem analytically tractable (Haggard and Cowan 2018). Specular reflection from surface liquid water is important as it is a direct indication of habitability (Robinson et al. 2014, Robinson 2018). Combining Lambertian mapping at gibbous phases with glint mapping at crescent phases would provide strong evidence for surface liquids (Lustig-Yaeger et al. 2018): oceans appear dark at most phases, but bright when specularly reflecting grazing sunlight (especially in polarized light; Groot et al. 2020).

Occultations

If a planet passes directly behind its star, then one may map its day side. Eclipse mapping can be applied to either planetary emission or reflected light, but the contrast ratio makes the latter daunting. While the eclipse depth is proportional to the integrated dayside brightness of the planet, the detailed shape of ingress and egress is a function of the spatial distribution of flux on the planet's dayside (Fig. 3). Although eclipses of planets by their host star have so far garnered the most attention, occultations by moons or other planets are also possible, especially in packed planetary systems like TRAPPIST-1 (Veras and Breedt 2017; Luger et al. 2017).

Fast codes are now available to produce occultation lightcurves numerically (SPIDERMAN; Louden and Kreidberg 2018) and analytically (starry; Luger et al. 2019a). The sharp kernel edge during an occultation—the stellar limb—increases the spatial resolution achievable in eclipse maps, and a larger impact parameter provides better latitudinal resolution (Boone et al. 2023).

Current Results and Future Prospects

The atmospheres of a few dozen exoplanets have been mapped via their thermal phase curves, e.g., the ExoAtmospheres and exoplanet.edu databases. These phase measurements have so far been mostly IRAC photometry from the Spitzer Space
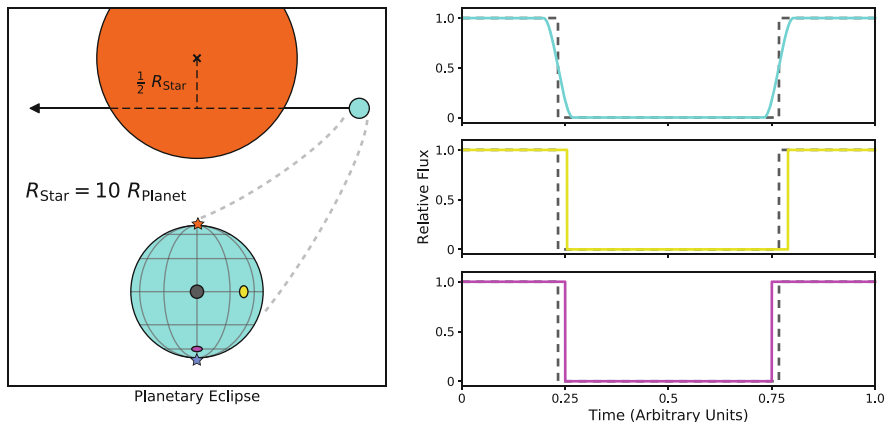
Fig. 3 Schematic showing the dominant signals present in secondary eclipse lightcurves. The teal lightcurve denotes a uniform planet (Mandel and Agol 2002). The gray dashed line is the eclipse shape if the planetary flux is concentrated in the center of the disk (a caricature of limb darkening or the dayside hot spot of a short-period planet; Rauscher et al. 2007) The yellow and magenta lines show the lightcurves for the same concentrated bright spot at different locations on the planetary disk. In particular, the yellow line shows the effect of a longitudinal offset predicted by Williams et al. (2006) and measured by Agol et al. (2010). The magenta line shows the effect of a latitudinal offset predicted by Rauscher et al. (2007) and measured by Majeau et al. (2012) and de Wit et al. (2012). All of these signals suffer degeneracies with system geometry, notably impact parameter, planet/star radius ratio, and orbital eccentricity; ancillary constraints are therefore crucial to eclipse mapping (de Wit et al. 2012; Rauscher et al. 2018). Moreover, some degeneracies can be lifted with spectrally resolved data (Dobbs-Dixon et al. 2015): the planetary map may be wavelength-dependent, but the system geometry cannot. (Figure from J.C. Schwartz (private communication))

Telescope (e.g., Bell et al. 2021; May et al. 2022; Dang et al. 2024), or spectroscopy with the Hubble Space Telescope's WFC3 (e.g., Stevenson et al. 2014; Kreidberg et al. 2018). The interested reader is pointed to the brief history of thermal phase curves in Charnay et al. (2022). Phase measurements from the James Webb Space Telescope have started being published, but so far focusing primarily on photometry (Mikal-Evans et al. 2023; Kempton et al. 2023; Bell et al. 2024). Rotational phase variations of brown dwarfs have also been measured and converted into brightness maps (e.g., Apai et al. 2017; Artigau 2018).

The Ariel mission could measure spectroscopic phase curves for dozens—if not hundreds—of planets and brown dwarfs (Charnay et al. 2022). The wavelength coverage of *Ariel* and JWST should be able to discriminate between thermal emission and reflected light (Schwartz and Cowan 2015; Parmentier et al. 2016; Keating and Cowan 2017), as well as disentangling phase variations, star spots, Doppler beaming, ellipsoidal variations, and gas accretion (Cowan et al. 2012a; Knutson et al. 2012; Esteves et al. 2015; Dang et al. 2018; Bell et al. 2019).

Eclipse mapping of hot Jupiters has so far been performed with *Spitzer*/IRAC photometry (Majeau et al. 2012; de Wit et al. 2012) and JWST/NIRISS spectroscopy
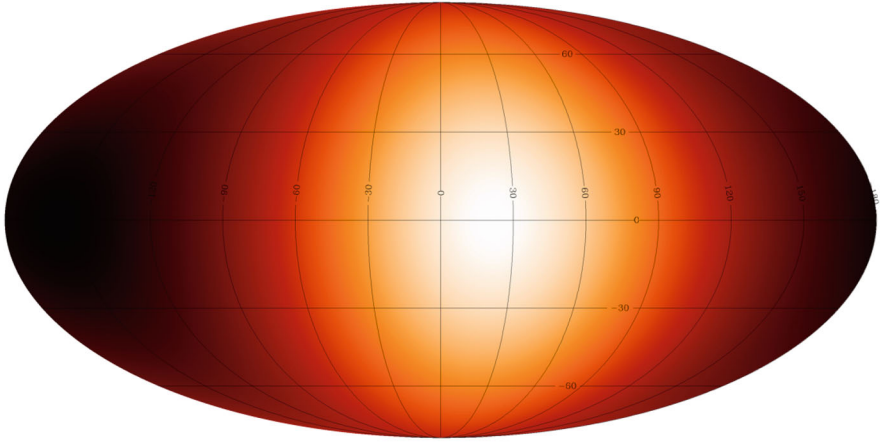
Fig. 4 Two-dimensional thermal map of the hot Jupiter HD 189733b, based on mid-infrared phase and eclipse measurements from the Spitzer Space Telescope (from Majeau et al. 2012). The substellar point is in the center of the map. The equatorial hotspot indicates a small obliquity, while the eastward offset is probably due to super-rotating zonal winds (Showman and Guillot 2002)

(Coulombe et al. 2023), though Hammond et al. (2024) contend that the eclipse mapping signal has thus far been marginal. Figure 4 shows the combined phase+eclipse map of HD 189733b from Majeau et al. (2012) showing both longitudinal and latitudinal information, making this a coarse 2D map. The high signal-to-noise and spectral resolution of JWST should enable 3D temperature maps of the daysides of hot Jupiters, and 2D (longitude and altitude) temperature maps of their nightsides. Eclipse mapping of longer-period planets, which may not be tidally locked, could reveal their spin axis (Rauscher 2017; Adams and Rauscher 2023; Rauscher et al. 2023).

Ground-based direct imaging could detect variations in thermal emission from directly imaged planets due to rotation of patchy clouds in and out of view (Biller et al. 2021), as is currently performed for brown dwarfs. The next generation of ground-based telescopes should enable both photometric mapping and Doppler tomography of giant planets (Crossfield et al. 2014), while the Large Interferometer for Exoplanets (Quanz et al. 2022) could map the climates of temperate terrestrial planets (e.g., Gaidos and Williams 2004; Cowan et al. 2012b; Mettler et al. 2023).

Demory et al. (2013) constructed an albedo map of the hot Jupiter Kepler-7b based on phase curves from the Kepler mission (Fig. 5). NASA's Grace Roman Space Telescope will directly image Jupiter analogs in reflected light, hence enabling rotational mapping of their clouds. The Habitable Worlds Observatory will enable reflected light surface mapping and spin determination for terrestrial planets (Figure 6; Ford et al. 2001; Pallé et al. 2008; Oakley and Cash 2009; Cowan et al.
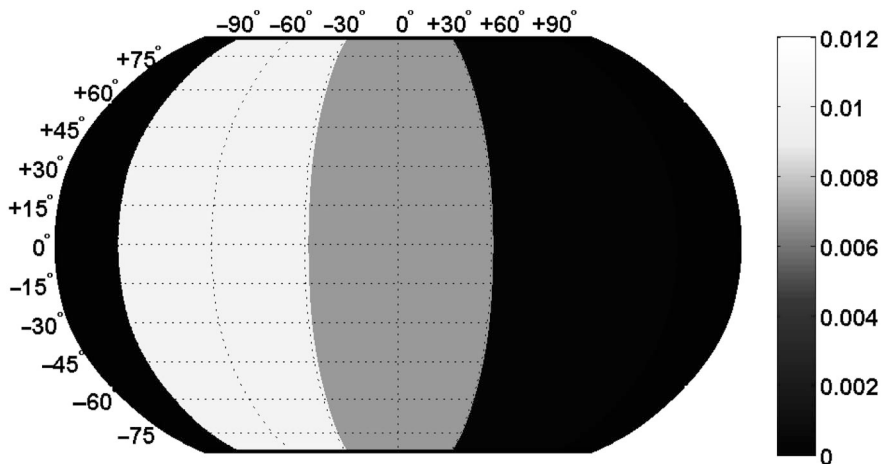
Fig. 5 Map of normalized intensity, I_p/I_*, for the planet Kepler-7b based on orbital phase variations measured by the Kepler mission (Adapted from Demory et al. 2013). The intensity is interpreted as reflected light and hence is proportional to albedo, $A_g = (I_p/I_*)(a/R_*)^2$, and the bright region on the planet's western hemisphere has an albedo of 0.64, suggestive of reflective clouds (Sudarsky et al. 2000; Roman and Rauscher 2017). A possible explanation for the cloud pattern is that particles condense on the planet's cooler nightside, are advected to the dayside by eastward winds, and sublimate when the star is overhead (Heng and Demory 2013; Parmentier et al. 2016)

2009, 2011; Kawahara and Fujii 2010, 2011; Fujii and Kawahara 2012; Cowan and Strait 2013; Schwartz et al. 2016; Kawahara 2016; Fujii et al. 2017; Jiang et al. 2018; Farr et al. 2018; Luger et al. 2019b; Fan et al. 2019; Kawahara 2020; Aizawa et al. 2020; Nakagawa et al. 2020).

Surface water is the definition of planetary habitability (Kasting et al. 1993), while the bimodal surface character of Earth—large oceans and exposed continents—may be crucial to its long-term habitability (Walker et al. 1981; Abbot et al. 2012; Foley 2015, 2019; Dorn et al. 2018; Foley and Smye 2018; Höning et al. 2019). Constructing surface maps of terrestrial exoplanets will therefore be a step toward understanding habitable environments outside of the Solar System and indeed to finding inhabited worlds (for a review see Suto 2019).

Clouds are a blessing and a curse to exo-cartography. From Earth to brown dwarfs, clouds contribute to the spatial inhomogeneity that makes exo-cartography interesting and feasible. But clouds also mask underlying features and often vary in time. Ongoing efforts are demonstrating how to map clouds and devising schemes to minimize their effects (Cowan et al. 2009; Cowan and Strait 2013; Fujii et al. 2017; Jiang et al. 2018) in order to catch glimpses of the planetary surface below (Kawahara and Masuda 2020; Teinturier et al. 2022).
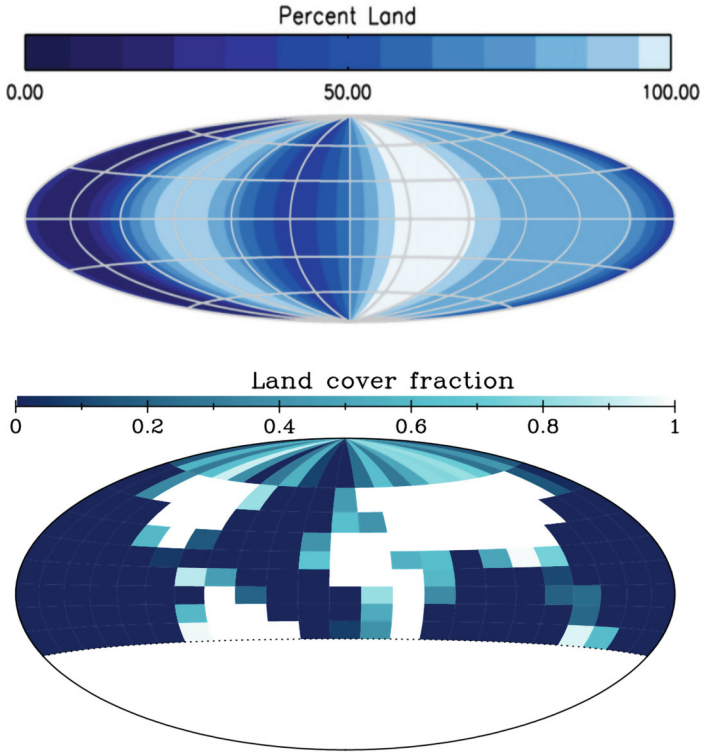
Fig. 6 *Top:* A one-dimensional color map of Earth based on 24 hours of disk-integrated photometry obtained by the Deep Impact spacecraft as part of the EPOXI mission (from Cowan et al. 2009). *Bottom:* A two-dimensional surface map recovered from simulated full-orbit multiband observations of a cloud-free Earth twin (from Kawahara and Fujii 2010); in this simulation, the observer was at northern latitudes and hence could not map the southern portion of the planet. One can readily identify the major landforms and oceans in either of these maps, unambiguously identifying this planet as habitable. Most reflected light mapping studies have validated their methods using Earth-as-an-exoplanet (Robinson and Reinhard 2020)

Cross-References

References

Abbot DS, Cowan NB, Ciesla FJ (2012) Indication of insensitivity of planetary weathering behavior and habitable zone to surface land fraction. ApJ 756:178

Adams AD, Rauscher E (2023) The sensitivity of eclipse mapping to planetary rotation. AJ 165(1):24

Agol E, Cowan NB, Knutson HA et al (2010) The climate of HD 189733b from fourteen transits and eclipses measured by Spitzer. ApJ 721:1861–1877

Aizawa M, Kawahara H, Fan S (2020) Global mapping of an exo-Earth using sparse modeling. ApJ 896(1):22

Apai D, Karalidi T, Marley MS et al (2017) Zones, spots, and planetary-scale waves beating in brown dwarf atmospheres. Science 357(6352):683–687

Beatty TG, Marley MS, Gaudi BS et al (2019) Spitzer phase curves of KELT-1b and the signatures of nightside clouds in thermal phase observations. AJ 158(4):166

Bell TJ, Zhang M, Cubillos PE et al (2019) Mass loss from the exoplanet WASP-12b inferred from Spitzer phase curves. MNRAS 489(2):1995–2013

Bell TJ, Dang L, Cowan NB et al (2021) A comprehensive reanalysis of Spitzer's 4.5 µm phase curves, and the phase variations of the ultra-hot Jupiters MASCARA-1b and KELT-16b. MNRAS 504(3):3316–3337

Bell et al (2024) https://ui.adsabs.harvard.edu/abs/2024NatAs...8..879B/abstract

Biller BA, Apai D, Bonnefoy M et al (2021) A high-contrast search for variability in HR 8799bc with VLT-SPHERE. MNRAS 503(1):743–767

Boone S, Grant D, Hammond M (2023) An analytic theory for the resolution attainable using eclipse mapping of exoplanets. arXiv e-prints arXiv:2310.14245. https://ui.adsabs.harvard.edu/abs/2024MNRAS.528..596B/abstract

Boucher A, Lafreniére D, Pelletier S et al (2023) CO or no CO? Narrowing the CO abundance constraint and recovering the H_2O detection in the atmosphere of WASP-127 b using SPIRou. MNRAS 522(4):5062–5083

Brogi M, Snellen IAG, de Kok RJ et al (2012) The signature of orbital motion from the dayside of the planet τ Boötis b. Nature 486(7404):502–504

Buenzli E, Apai D, Radigan J, Reid IN Flateau D (2014) Brown Dwarf photospheres are patchy: a hubble space telescope near-infrared spectroscopic survey finds frequent low-level variability. ApJ 782:77

Challener RC, Rauscher E (2023) The eclipse-mapping null space: comparing theoretical predictions with observed maps. AJ 166(4):176

Changeat Q, Al-Refaie A (2020) TauREx3 PhaseCurve: a 1.5D model for phase-curve description. ApJ 898(2):155

Charbonneau D, Allen LE, Megeath ST et al (2005) Detection of thermal emission from an extrasolar planet. ApJ 626:523–529

Charnay B, Mendonça JM, Kreidberg L et al (2022) A survey of exoplanet phase curves with Ariel. Exp Astron 53(2):417–446

Coulombe LP, Benneke B, Challener R et al (2023) A broadband thermal emission spectrum of the ultra-hot Jupiter WASP-18b. Nature 620(7973):292–298

Cowan NB, Agol E (2008) Inverting phase functions to map exoplanets. ApJ 678: L129–L132

Cowan NB, Strait TE (2013) Determining reflectance spectra of surfaces and clouds on exoplanets. ApJ 765:L17

Cowan NB, Agol E, Meadows VS et al (2009) Alien maps of an ocean-bearing world. ApJ 700:915–923

Cowan NB, Robinson T, Livengood TA et al (2011) Rotational variability of Earth's polar regions: implications for detecting snowball planets. ApJ 731:76

Cowan NB, Machalek P, Croll B et al (2012a) Thermal phase variations of WASP-12b: defying predictions. ApJ 747:82

Cowan NB, Voigt A, Abbot DS (2012b) Thermal phases of Earth-like planets: estimating thermal inertia from eccentricity, obliquity, and diurnal forcing. ApJ 757(1):80

Cowan NB, Fuentes PA, Haggard HM (2013) Light curves of stars and exoplanets: estimating inclination, obliquity and albedo. MNRAS 434:2465–2479

Cowan NB, Chayes V, Bouffard É, Meynig M, Haggard HM (2017) Odd harmonics in exoplanet photometry: weather or artifact? MNRAS 467:747–757

Crossfield IJM, Biller B, Schlieder JE et al (2014) A global cloud map of the nearest known brown dwarf. Nature 505:654–656

Cubillos PE, Keating D, Cowan NB et al (2021) Longitudinally resolved spectral retrieval (ReSpect) of WASP-43b. ApJ 915(1):45

Dang L, Cowan NB, Schwartz JC et al (2018) Detection of a westward hotspot offset in the atmosphere of hot gas giant CoRoT-2b. Nat Astron 2:220–227

Dang L, Bell TJ, Cowan NB et al (2022) Thermal phase curves of XO-3b: an eccentric hot Jupiter at the deuterium burning limit. AJ 163(1):32

Dang et al (2024) https://ui.adsabs.harvard.edu/abs/2024arXiv240813308D/abstract

de Wit J, Gillon M, Demory BO, Seager S (2012) Towards consistent mapping of distant worlds: secondary-eclipse scanning of the exoplanet HD 189733b. A&A 548:A128

de Wit J, Lewis NK, Langton J et al (2016) Direct measure of radiative and dynamical properties of an exoplanet atmosphere. ApJ 820(2):L33

Deming D, Seager S, Richardson LJ, Harrington J (2005) Infrared radiation from an extrasolar planet. Nature 434:740–743

Demory BO, de Wit J, Lewis N et al (2013) Inference of inhomogeneous clouds in an exoplanet atmosphere. ApJ 776:L25

Dobbs-Dixon I, Agol E, Burrows A (2012) The impact of circumplantary jets on transit spectra and timing offsets for hot Jupiters. ApJ 751:87

Dobbs-Dixon I, Agol E, Deming D (2015) Spectral eclipse timing. ApJ 815:60

Dorn C, Noack L, Rozel AB (2018) Outgassing on stagnant-lid super-Earths. A&A 614:A18

Ehrenreich D, Lovis C, Allart R et al (2020) Nightside condensation of iron in an ultrahot giant exoplanet. Nature 580(7805):597–601

Espinoza N, Jones K (2021) Constraining mornings and evenings on distant worlds: a new semianalytical approach and prospects with transmission spectroscopy. AJ 162(4):165

Esteves LJ, De Mooij EJN, Jayawardhana R (2015) Changing phases of alien worlds: probing atmospheres of Kepler planets with high-precision photometry. ApJ 804:150

Fan S, Li C, Li JZ et al (2019) Earth as an exoplanet: a two-dimensional alien map. ApJ 882(1):L1

Farr B, Farr WM, Cowan NB, Haggard HM, Robinson T (2018) exocartographer: a Bayesian framework for mapping exoplanets in reflected light. AJ 156(4):146

Feng YK, Line MR, Fortney JJ et al (2016) The impact of non-uniform thermal structure on the interpretation of exoplanet emission spectra. ApJ 829(1):52

Foley BJ (2015) The role of plate tectonic-climate coupling and exposed land area in the development of habitable climates on rocky planets. ApJ 812:36

Foley BJ (2019) Habitability of Earth-like stagnant lid planets: climate evolution and recovery from snowball states. ApJ 875(1):72

Foley BJ, Smye AJ (2018) Carbon cycling and habitability of Earth-sized stagnant lid planets. Astrobiology 18(7):873–896

Ford EB, Seager S, Turner EL (2001) Characterization of extrasolar terrestrial planets from diurnal photometric variability. Nature 412:885–887

Fujii Y, Kawahara H (2012) Mapping Earth analogs from photometric variability: spin-orbit tomography for planets in inclined orbits. ApJ 755:101

Fujii Y, Kawahara H, Suto Y et al (2010) Colors of a second Earth: estimating the fractional areas of ocean, land, and vegetation of Earth-like exoplanets. ApJ 715:866–880

Fujii Y, Kawahara H, Suto Y et al (2011) Colors of a second Earth. II. Effects of clouds on photometric characterization of Earth-like exoplanets. ApJ 738:184

Fujii Y, Lustig-Yaeger J, Cowan NB (2017) Rotational spectral unmixing of exoplanets: degeneracies between surface colors and geography. AJ 154(5):189

Gaidos E, Williams DM (2004) Seasonality on terrestrial extrasolar planets: inferring obliquity and surface conditions from infrared light curves. New A 10:67–77

Gómez-Leal I, Pallé E, Selsis F (2012) Photometric variability of the disk-integrated thermal emission of the Earth. ApJ 752:28

Grant D, Wakeford HR (2023) Transmission strings: a technique for spatially mapping exoplanet atmospheres around their terminators. MNRAS 519(4):5114–5127

Groot A, Rossi L, Trees VJH, Cheung JCY, Stam DM (2020) Colors of an Earth-like exoplanet. Temporal flux and polarization signals of the Earth. A&A 640:A121

Haggard HM, Cowan NB (2018) Analytic reflected light curves for exoplanets. MNRAS 478(1):371–385

Hammond et al (2024) https://ui.adsabs.harvard.edu/abs/2024MNRAS.532.4350H/abstract

Heng K, Demory BO (2013) Understanding trends associated with clouds in irradiated exoplanets. ApJ 777:100

Höning D, Tosi N, Spohn T (2019) Carbon cycling and interior evolution of water-covered plate tectonics and stagnant-lid planets. A&A 627:A48

Irwin PGJ, Parmentier V, Taylor J et al (2020) 2.5D retrieval of atmospheric properties from exoplanet phase curves: application to WASP-43b observations. MNRAS 493(1):106–125

Jiang JH, Zhai AJ, Herman J et al (2018) Using deep space climate observatory measurements to study the Earth as an exoplanet. AJ 156(1):26

Kasting JF, Whitmire DP, Reynolds RT (1993) Habitable zones around main sequence stars. Icarus 101:108–128

Kawahara H (2016) Frequency modulation of directly imaged exoplanets: geometric effect as a probe of planetary obliquity. ApJ 822:112

Kawahara H (2020) Global mapping of the surface composition on an exo-Earth using color variability. ApJ 894(1):58

Kawahara H, Fujii Y (2010) Global mapping of Earth-like exoplanets from scattered light curves. ApJ 720:1333–1350

Kawahara H, Fujii Y (2011) Mapping clouds and terrain of Earth-like planets from photometric variability: demonstration with planets in face-on orbits. ApJ 739:L62

Kawahara H, Masuda K (2020) Bayesian dynamic mapping of an exo-Earth from photometric variability. ApJ 900(1):48

Keating D, Cowan NB (2017) Revisiting the energy budget of WASP-43b: enhanced day-night heat transport. ApJ 849(1):L5

Keating D, Cowan NB, Dang L (2019) Uniformly hot nightside temperatures on short-period gas giants. Nat Astron 3:1092–1098

Kempton EMR, Bean JL, Parmentier V (2017) An observational diagnostic for distinguishing between clouds and haze in hot exoplanet atmospheres. ApJ 845(2):L20

Kempton EMR, Zhang M, Bean JL et al (2023) A reflective, metal-rich atmosphere for GJ 1214b from its JWST phase curve. Nature 620(7972):67–71

Klein et al (2024) https://ui.adsabs.harvard.edu/abs/2024MNRAS.527..544K/abstract

Knutson HA, Charbonneau D, Allen LE et al (2007) A map of the day-night contrast of the extrasolar planet HD 189733b. Nature 447:183–186

Knutson HA, Lewis N, Fortney JJ et al (2012) 3.6 and 4.5 µm phase curves and evidence for non-equilibrium chemistry in the atmosphere of extrasolar planet HD 189733b. ApJ 754:22

Kostov V, Apai D (2013) Mapping directly imaged giant exoplanets. ApJ 762:47

Kreidberg L, Line MR, Parmentier V et al (2018) Global climate and atmospheric composition of the ultra-hot Jupiter WASP-103b from HST and Spitzer phase curve observations. AJ 156(1):17

Lewis NK, Knutson HA, Showman AP et al (2013) Orbital phase variations of the eccentric giant planet HAT-P-2b. ApJ 766:95

Louden T, Kreidberg L (2018) SPIDERMAN: an open-source code to model phase curves and secondary eclipses. MNRAS 477(2):2613–2627

Louden T, Wheatley PJ (2015) Spatially resolved eastward winds and rotation of HD 189733b. ApJ 814:L24

Luger R, Lustig-Yaeger J, Agol E (2017) Planet-planet occultations in TRAPPIST-1 and other exoplanet systems. ApJ 851(2):94

Luger R, Agol E, Foreman-Mackey D et al (2019a) starry: analytic occultation light curves. AJ 157(2):64

Luger R, Bedell M, Vanderspek R, Burke CJ (2019b) TESS photometric mapping of a terrestrial planet in the habitable zone: detection of clouds, oceans, and continents. arXiv e-prints arXiv:1903.12182

Luger R, Foreman-Mackey D, Hedges C (2021) starry_process: interpretable Gaussian processes for stellar light curves. J Open Source Softw 6(63):3071

Luger R, Agol E, Bartolić F, Foreman-Mackey D (2022) Analytic light curves in reflected light: phase curves, occultations, and non-Lambertian scattering for spherical planets and moons. AJ 164(1):4

Lustig-Yaeger J, Meadows VS, Tovar Mendoza G et al (2018) Detecting ocean glint on exoplanets using multiphase mapping. AJ 156(6):301

MacDonald RJ, Lewis NK (2022) TRIDENT: a rapid 3D radiative-transfer model for exoplanet transmission spectra. ApJ 929(1):20

Majeau C, Agol E, Cowan NB (2012) A two-dimensional infrared map of the extrasolar planet HD 189733b. ApJ 747:L20

Mandel K, Agol E (2002) Analytic light curves for planetary transit searches. ApJ 580:L171–L175

Marois C, Macintosh B, Barman T et al (2008) Direct imaging of multiple planets orbiting the star HR 8799. Science 322:1348–1352

May EM, Stevenson KB, Bean JL et al (2022) A new analysis of eight Spitzer phase curves and hot Jupiter population trends: Qatar-1b, Qatar-2b, WASP-52b, WASP-34b, and WASP-140b. AJ 163(6):256

McTier MAS, Kipping DM (2018) Finding mountains with molehills: the detectability of exotopography. MNRAS 475(4):4978–4985

Mettler JN, Quanz SP, Helled R, Olson SL, Schwieterman EW (2023) Earth as an exoplanet. II. Earth's time-variable thermal emission and its atmospheric seasonality of bioindicators. ApJ 946(2):82

Mikal-Evans T, Sing DK, Dong J et al (2023) A JWST NIRSpec phase curve for WASP-121b: dayside emission strongest eastward of the substellar point and nightside conditions conducive to cloud formation. ApJ 943(2):L17

Nakagawa Y, Kodama T, Ishiwatari M et al (2020) Obliquity of an Earth-like planet from frequency modulation of its direct-imaged lightcurve: mock analysis from general circulation model simulation. ApJ 898(2):95

Nguyen TG, Cowan NB, Banerjee A, Moores JE (2020) Modelling the atmosphere of lava planet K2-141b: implications for low- and high-resolution spectroscopy. MNRAS 499(4): 4605–4612

Oakley PHH, Cash W (2009) Construction of an Earth model: analysis of exoplanet light curves and mapping the next Earth with the new worlds observer. ApJ 700:1428–1439

Pallé E, Ford EB, Seager S, Montañés-Rodríguez P, Vazquez M (2008) Identifying the rotation rate and the presence of dynamic weather on extrasolar Earth-like planets from photometric observations. ApJ 676:1319–1329

Parmentier V, Fortney JJ, Showman AP, Morley C, Marley MS (2016) Transitions in the cloud composition of hot Jupiters. ApJ 828:22

Powell D, Louden T, Kreidberg L et al (2019) Transit signatures of inhomogeneous clouds on hot Jupiters: insights from microphysical cloud modeling. ApJ 887(2):170

Quanz SP, Ottiger M, Fontanet E et al (2022) Large Interferometer For Exoplanets (LIFE). I. Improved exoplanet detection yield estimates for a large mid-infrared space-interferometer mission. A&A 664:A21

Rauscher E (2017) Models of warm Jupiter atmospheres: observable signatures of obliquity. ApJ 846(1):69

Rauscher E, Menou K, Seager S et al (2007) Toward eclipse mapping of hot Jupiters. ApJ 664:1199–1209

Rauscher E, Suri V, Cowan NB (2018) A more informative map: inverting thermal orbital phase and eclipse light curves of exoplanets. AJ 156(5):235

Rauscher E, Cowan NB, Luger R (2023) Warm Jupiters beyond the tidal synchronization limit may exhibit a wide range of secondary eclipse depths. AJ 165(6):261

Robinson TD, Reinhard CT (2020) Earth as an exoplanet. In: Meadows VS, Arney GN, Schmidt BE, Des Marais DJ (eds) Planetary astrobiology, p 379. https://doi.org/10.2458/azu_uapress_9780816540068

Robinson TD, Meadows VS, Crisp D (2010) Detecting oceans on extrasolar planets using the glint effect. ApJ 721:L67–L71

Robinson TD, Meadows VS, Crisp D et al (2011) Earth as an extrasolar planet: Earth model validation using EPOXI Earth observations. Astrobiology 11:393–408

Robinson TD, Ennico K, Meadows VS et al (2014) Detection of ocean glint and ozone absorption using LCROSS Earth observations. ApJ 787:171

Roman M, Rauscher E (2017) Modeling the effects of inhomogeneous aerosols on the hot Jupiter Kepler-7b's atmospheric circulation. ApJ 850(1):17

Russell HN (1906) On the light variations of asteroids and satellites. ApJ 24:1–18

Schwartz JC, Cowan NB (2015) Balancing the energy budget of short-period giant planets: evidence for reflective clouds and optical absorbers. MNRAS 449:4192–4203

Schwartz JC, Sekowski C, Haggard HM, Pallé E, Cowan NB (2016) Inferring planetary obliquity using rotational and orbital photometry. MNRAS 457:926–938

Showman AP, Guillot T (2002) Atmospheric circulation and tides of "51 Pegasus b-like" planets. A&A 385:166–180

Stevenson KB, Désert JM, Line MR et al (2014) Thermal structure of an exoplanet atmosphere from phase-resolved emission spectroscopy. Science 346:838–841

Sudarsky D, Burrows A, Pinto P (2000) Albedo and reflection spectra of extrasolar giant planets. ApJ 538:885–903

Suto Y (2019) How to search for possible bio-signatures on Earth-like planets: beyond a pale blue dot. In: Yamagishi A, Kakegawa T, Usui T (eds) Astrobiology, p 441. https://doi.org/10.1007/978-981-13-3639-3_29

Teinturier L, Vieira N, Jacquet E et al (2022) Mapping the surface of partially cloudy exoplanets is hard. MNRAS 511(1):440–447

Toth VT, Turyshev SG (2023) Imaging rotating and orbiting exoplanets with the solar gravitational lens. MNRAS 525(4):5846–5856

Vanderburg A, Rappaport SA, Xu S et al (2020) A giant planet candidate transiting a white dwarf. Nature 585(7825):363–367

Veras D, Breedt E (2017) Eclipse, transit and occultation geometry of planetary systems at exo-syzygy. MNRAS 468:2672–2683

Walker JCG, Hays PB, Kasting JF (1981) A negative feedback mechanism for the long-term stabilization of the Earth's surface temperature. J Geophys Res 86:9776–9782

Wiktorowicz SJ, Stam DM (2015) Exoplanets, p 439

Williams PKG, Charbonneau D, Cooper CS, Showman AP, Fortney JJ (2006) Resolving the surfaces of extrasolar planets with secondary eclipse light curves. ApJ 649:1020–1027

Zhang X (2023a) The inhomogeneity effect. I. Inhomogeneous surface and atmosphere accelerate planetary cooling. ApJ 957(1):20

Zhang X (2023b) The inhomogeneity effect. II. Rotational and orbital states impact planetary cooling. ApJ 957(1):21

Zhang X, Li C, Ge H, Le T (2023) The inhomogeneity effect. III. Weather impacts on the heat flow of hot Jupiters. ApJ 957(1):22